Journal of Sound and Vibration (1994) **170**(2), 237–259

FREE VIBRATIONS OF BEAMS WITH A SINGLE-EDGE CRACK

M.-H. H. SHEN

Department of Aeronautical and Astronautical Engineering, The Ohio State University, Columbus, Ohio 43210-1276, *U.S.A.*

AND

C. PIERRE

Department of Mechanical Engineering and Applied Mechanics, The University of Michigan, Ann Arbor, Michigan 48109-2125, *U.S.A.*

(*Received* 21 *May* 1990, *and in final form* 14 *August* 1992)

The equation of motion and associated boundary conditions are derived for a uniform Bernoulli–Euler beam containing one single-edge crack. The generalized variational principle used allows for modified stress, strain and displacement fields that satisfy the compatibility requirements in the vicinity of the crack. The concentration in stress is represented by introducing a crack function into the beam's compatibility relations. A displacement function is also introduced to modify the in-plane displacement and its slope near the crack. Both functions are chosen to have their maximum value at the cracked section and to decay exponentially along the beam's longitudinal direction. The rate of exponential decay is evaluated from finite element calculations. The resulting equation of motion is solved for simply supported and cantilevered beams with single-edge cracks by a Galerkin and a local Ritz procedure, respectively. These theoretical natural frequencies and mode shapes match closely with experimental and finite element results. The possibility of determining the damage properties of cracked beams from changes in dynamic behavior is discussed.

1. INTRODUCTION

The development of damage identification techniques for vibrating structures such as turbines, generators, motors, aircraft structures and large space structures has recently become a focus of substantially growing research efforts. Due to increasing demands for safety, reliability and time-efficiency, it is now believed that the monitoring of the global dynamics of a structure offers promising alternatives for damage detection. Consequently, the study of the dynamics of cracked structures is of importance.

Several investigators have examined the dynamics of cracked structures. For example, the effects of cracks on the dynamic behavior of beams was studied by Chondros and Dimarogonas [1], Dimarogonas and Massouros [2] and Dimarogonas and Papadopoulos [3]. They modelled the crack by introducing a local flexibility matrix connecting longitudinal, bending and shear forces and displacements. Later, Gudmundson [4] and several other researchers generalized this idea to a 6×6 flexibility matrix relating all six generalized forces to the corresponding displacements, and applied it to a variety of dynamic problems. Torsion was also considered by Papadopoulos and Dimarogonas [5], who derived a more complete flexibility matrix. They showed that a crack in a Timoshenko shaft introduces coupling between torsion and shear. Since, in the Timoshenko beam model, there is

0022-460X/94/070237 + 23 $08.00/0

coupling between the shear and bending deformations, the torsional motion is coupled to the bending one for a cracked shaft.

Cawley and Adams [6, 7] demonstrated the feasibility of using natural frequency test measurements to detect damage in a structure. Their approach consisted of comparing the natural frequencies obtained from finite element analysis with the measured frequencies. They introduced damage in the finite element model by a reduced stiffness element. The damage location was determined by replacing each element with a reduced stiffness element until the finite frequencies matched best the measured frequencies.

Recently, Christides and Barr [8] derived the equations of bending motion for a Bernoulli–Euler beam containing pairs of symmetric cracks. The cracks were taken to be normal to the beam's neutral axis and symmetrical about the plane of bending. They used an exponential-type function (the so-called "crack function") to model the stress concentration near the crack tip. The rate of stress decay from the crack was controlled by a dimensionless parameter, α, that was determined by fitting the analytical results to experimental data. However, Christides and Barr obtained the approximate cracked beam natural frequencies by a two-term Rayleigh–Ritz procedure. Recently, Shen and Pierre [9] showed that this two-term solution does not feature adequate convergence and that, indeed, convergence is very slow for this type of problems, because cracks affect the continuity characteristics of the solution. To ensure adequate convergence, an approximate Galerkin solution with as many as 150 terms was suggested in reference [9], which led to a redetermination of the stress decay rate α. To validate the theoretical results, a two-dimensional finite element approach was also proposed in reference [9], which allows one to determine α without requiring the use of experimental results.

The cracked beam theory in references [8, 9] is restricted to pairs of symmetric cracks. This assumption was made to avoid the modelling difficulty due to the discontinuities in the slope of the neutral axis and in the axial displacement along the neutral axis, which both occur with a non-symmetric crack configuration. Furthermore, in order to avoid the non-linear characteristics occurred by allowing crack face contacts during the vibration, the crack was assumed open in the cracked beam theory. The crack beam theory of references [8] and [9] is further extended in the present study, which investigates the effects of *single* surface cracks on the modes of free vibration of beams. The analysis proceeds in several steps. First, we assume that the damage can be viewed as a single surface crack normal to the beam's neutral axis. According to the observations of Freund [10–12], Bodner [13] and Freund and Herrmann [14], that the normal stress distribution on the prospective fracture plane is essentially linear before initiation of the fracture on the tensile side of the beam, a crack function f is introduced into the normal stress and strain expressions to account for this phenomenon. Also, a function is introduced in the representation of the in-plane displacement to model the disruption of the deformation field due to the crack. A generalized variational principle extended from the Hu–Washizu principle is used to derive the governing equations for a uniform beam with a single-edge crack. This procedure is similar to that used for beams with pairs of symmetric cracks [8, 9]. These equations and boundary conditions are particularized for a cracked beam with rectangular cross-section. The Galerkin and Ritz methods are then applied to predict the free vibration modes of cracked beams, for simply supported and cantilevered configurations. The value of the stress decay factor α is determined by a least square fit of the natural frequencies calculated by Galerkin or Ritz methods with finite element results. For the cantilevered beam, a comparison with published experimental results is performed, and excellent agreement is observed.

Two basic issues are addressed in this study. First, the adequacy of a model based on a simple beam theory for the prediction of the dynamic response of cracked beams is

demonstrated. Second, the effects of a single surface crack on the free response of simply supported and cantilevered beams are investigated. The possible use of this formulation to identify the crack position and size from changes in the beams' natural frequencies and mode shapes is also discussed.

2. CRACKED BEAM THEORY FOR SINGLE-EDGE CRACKS

2.1. KINEMATIC ASSUMPTIONS

The distribution of stress and strain in an elastic body with a crack has been studied by Irwin [15] and Paris and Sih [16]. They divided the stress fields near the crack tip into three basic types, each associated with a local mode of deformation. These are mode I, the crack-edge opening mode; mode II, the crack-edge sliding mode; and mode III, the crack-edge tearing mode.

In the case of free bending vibrations of a uniform beam with a single-edge crack, the bending moment and the longitudinal force do not contribute to mode II and mode III deformations. The shear force does contribute to mode II deformation. However, for slender beams, this contribution can be neglected.

Similar to the case of symmetric cracks, the normal stress, σ_{xx}, is the only stress affected by a single crack. The remaining normal and shear stresses out of the plane of bending are assumed to be zero. The in-plane shear stress component, σ_{xz}, is included to accommodate the possibility of shear loading on the lateral surfaces of the beam. Since σ_{xz} is not concentrated in mode I, the details of its distribution are not affected by the crack.

In references [15] and [16], the normal stress σ_{xx} was found to be concentrated at the crack tip and to decay in inverse proportion to the square root of the distance from the crack tip. This phenomenon is reproduced here by using a crack function $f(x, z)$ in the expressions of the stress σ_{xx} and the strain ϵ_{xx}, as follows:

$$\sigma_{xx}(x, z, t) = (-z + f(x, z))T(x, t), \qquad \epsilon_{xx}(x, z, t) = (-z + f(x, z))S(x, t), \quad (1, 2)$$

where $T(x, t)$ and $S(x, t)$ are defined as unknown stress and strain functions, respectively.

The function $f(x, z)$ is maximum at the crack tip. It is taken to decay exponentially along the length of the beam and to vary linearly through the depth of the uncracked portion of the beam, according to:

$$f(x, z) = [z - m(z + a/2)H((d - a) - z)] \exp[-\alpha|x - x_c|/d]. \quad (3)$$

Here, x_c, a and d represent the crack position, the crack length and half the depth of the uncracked section, respectively, as shown in Figure 1. The positive non-dimensional constant α determines the rate of stress decay away from the crack tip. It was found to be 1·936 in reference [9] for a pair of symmetric cracks. At the crack section $x = x_c$ and for $z > (d - a)$ (i.e., within the crack), $f(x, z)$ reduces to z and the stress and strain in equations (1) and (2) are zero. The constant m represents the slope of the linear stress distribution at the cracked section (calculated in section 2.3).

The derivative of the axial displacement $u(x, z, t)$ is represented as

$$u'(x, z, t) = (-z + \varphi(x, z))w''(x, t), \quad (4)$$

where $w(x, t)$ is the transverse beam deflection. The function φ is chosen so that the surface of zero in-plane displacement coincides with the surface of zero normal stress. For (kinematic) consistancy between equations (2) and (4) we choose $\varphi(x, z)$ to be similar in form to $f(x, z)$ in equation (3):

$$\varphi(x, z) = [z - (z + a/2)H((d - a) - z)] \exp(-2\beta|x - x_c|d). \quad (5)$$

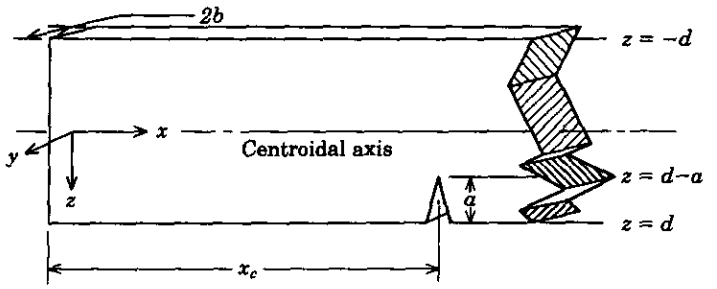

Figure 1. Geometry of a beam with a single-edge crack at x_c.

The assumptions for a nominally uniform beam with a single surface crack are summarized as

$$\begin{cases} u_x = u(x, z, t), \quad u_y = 0, \quad u_z = w(x, t), \\ p_x = 0, \quad p_y = 0, \quad p_z = P(x, t), \\ \epsilon_{xx} = (-z + f(x, z))S(x, t), \\ \epsilon_{yy} = \epsilon_{zz} = -\nu\epsilon_{xx}, \\ \epsilon_{xy} = \epsilon_{yz} = \epsilon_{xz} = 0, \\ \sigma_{xx} = (-z + f(x, z))T(x, t), \quad \sigma_{xz} = \sigma_{xz}(x, z, t), \\ \sigma_{yy} = \sigma_{zz} = \sigma_{xy} = \sigma_{yz} = 0, \\ X_x = X_y = X_z = 0, \end{cases} \tag{6}$$

where σ_{ij} and ϵ_{ij} are stress and strain components, and X_i and p_i are the body forces and velocity components, respectively. (The indices $i, j = 1, 2, 3$ refer to the orthogonal directions x, y, z, respectively.) The shear stress σ_{xz} is included to permit loading of the beam.

2.2. VARIATIONAL THEOREM

Since S, T, P and w are unknown functions, the compatibility and constitutive relations of the cracked beam are undefined. In the absence of these relations, classical variational principles such as Hamilton's principle are inadequate. However, these principles can be generalized by the introduction of Lagrange multipliers to yield a family of variational principles that includes the Hellinger–Reissner principle in elastodynamic problems and the Hu–Washizu principle in elastic static problems.

Here, the Hu–Washizu principle is modified to include the virtual work done by inertial forces. This yields the functional:

$$J = \int_{t_1}^{t_2} \left\{ \int_V [\rho p_i \dot{u}_i - \tfrac{1}{2}\rho p_i p_i - \underline{A}(\epsilon_{ij}) + (\epsilon_{ij} - \tfrac{1}{2}(u_{i,j} + u_{j,i}))\sigma_{ij} + X_i u_i] \, dV \right.$$
$$\left. + \int_{S_1} \bar{g}_i u_i \, dS_1 + \int_{S_2} g_i (u_i - \bar{u}_i) \, dS_2 \right\} dt, \tag{7}$$

where ρ is the density, $\underline{A}(\epsilon_{ij})$ is the strain energy density function, the g_i's are the surface tractions, V is the total volume of the system, and S its external surface. The overbarred quantities, $\bar{g}_i$ and $\bar{u}_i$ denote the prescribed values of surface tractions and surface displacements, respectively.

The functional J in equation (7) is stationary for the solution in the independent quantities u_i, p_i, ϵ_{ij} and σ_{ij}. Therefore, for arbitrary independent variations of δu_i (with conditions $\delta u_i(t_1) = \delta u_i(t_2) = 0$), δp_i, $\delta \epsilon_i$ and $\delta \sigma_i$, the first variation of J must be equal to zero, yielding

$$\delta J = \int_{t_1}^{t_2} \left\{ \int_V \{(\sigma_{ij,j} + X_i - \rho \dot{p}_i)\delta u_i + (\sigma_{ij} - \underline{A}_{,\epsilon_{ij}})\delta \epsilon_{ij} + [\epsilon_{ij} - \tfrac{1}{2}(u_{i,j} + u_{j,i})]\delta \sigma_{ij} + [\rho \dot{u}_i - (\tfrac{1}{2}\rho p_i p_i)_{,p_i}]\delta p_i \} \, dV + \int_{S_1} (\bar{g}_i - g_i)\delta u_i \, dS_1 + \int_{S_2} (u_i - \bar{u}_i)\delta g_i \, dS_2 \right\} dt = 0. \tag{8}$$

2.3. EQUATION OF MOTION AND ASSOCIATED BOUNDARY CONDITIONS

Assumptions (6) are substituted into the formulation (8), whereby the problem is reduced to a form corresponding to the beam model. After integration by parts and simplification, we obtain the following

2.3.1. *Strain–displacement term*

The strain–displacement term in equation (8) is

$$\int_V (\epsilon_{xx} - \partial u/\partial x)\delta \sigma_{xx} \, dV = \int_x \left\{ \int_A [(f - z)S - (\varphi - z)w'](f - z)\delta T \, dA \right\} dx. \tag{9}$$

Defining

$$I = \int_A z^2 \, dA, \qquad K = \int_A zf \, dA, \qquad L = \int_A f^2 \, dA,$$

$$K_1 = \int_A z\varphi \, dA, \qquad L_1 = \int_A f\varphi \, dA, \tag{10}$$

the right side of equation (9) can be written as

$$\int_x [(I - 2K + L)S - (I + L_1 - K - K_1)w']\delta T \, dx. \tag{11}$$

2.3.2. *Strain–stress term*

The strain–stress term in equation (8) is

$$\int_V \left[\left(\sigma_{xx} - \frac{\partial \underline{A}}{\partial \epsilon_{xx}} \right) \delta \epsilon_{xx} - \frac{\partial \underline{A}}{\partial \epsilon_{yy}} \delta \epsilon_{yy} - \frac{\partial \underline{A}}{\partial \epsilon_{zz}} \delta \epsilon_{zz} \right] dV. \tag{12}$$

If the material is elastic and isotropic, we have

$$\partial \underline{A}/\partial \epsilon_{xx} = E\epsilon_{xx}, \qquad \partial \underline{A}/\partial \epsilon_{yy} = 0, \qquad \partial \underline{A}/\partial \epsilon_{zz} = 0, \tag{13}$$

so equation (12) becomes

$$\int_V (\sigma_{xx} - E\epsilon_{xx})\delta \epsilon_{xx} \, dV = \int_x (T - ES)(I - 2K + L)\delta S \, dx. \tag{14}$$

2.3.3. *Velocity term*

The velocity term in equation (8) is

$$\int_x (\rho A\dot{w} - \rho PA)\delta P \, dx, \tag{15}$$

2.3.4. *Dynamic equilibrium term*

The first term in equation (8) represents the virtual work done by the dynamic forces. In the absence of body forces, it can be written as

$$\int_V \left\{ \frac{\partial \sigma_{xx}}{\partial x} \delta u + \frac{\partial \sigma_{xz}}{\partial z} \delta u + \left(\frac{\partial \sigma_{xz}}{\partial x} - \rho \dot{P} \right) \delta w \right\} \mathrm{d}V. \tag{16}$$

Under the assumptions (6), equation (16) becomes

$$\int_V \left\{ \left([(f-z)T]' + \frac{\partial \sigma_{xz}}{\partial z} \right) \varphi \delta w' - \left([(f-z)T]' + \frac{\partial \sigma_{xz}}{\partial z} \right) z \delta w' + \left(\frac{\partial \sigma_{xz}}{\partial x} - \rho \dot{P} \right) \delta w \right\} \mathrm{d}V, \tag{17}$$

Defining

$$K_2 = \int_A z\varphi' \, \mathrm{d}A, \qquad L_2 = \int_A f\varphi' \, \mathrm{d}A, \qquad L_3 = \int_A f'\varphi \, \mathrm{d}A,$$

$$L_4 = \int_A f''\varphi \, \mathrm{d}A, \qquad L_5 = \int_A f'\varphi' \, \mathrm{d}A, \tag{18}$$

and integrating by parts the first two terms in equation (17), we obtain

$$\int_A \left\{ [(f-z)T]' + \frac{\partial \sigma_{xz}}{\partial z} \right\} \partial \varphi w \, \mathrm{d}A \Big|_{x=0}^{x=l} - \int_y \int_x \frac{\partial (\varphi \sigma_{xz})}{\partial x} \delta w \, \mathrm{d}x \, \mathrm{d}y \Big|_{z=-d}^{z=d}$$

$$- \int_x \{(L_1 - K_1)T'' + 2T'L_3 + TL_4 + (L_2 - K_2)T' + L_5 T\} \delta w \, \mathrm{d}x. \tag{19}$$

Integrating by parts the last two terms of equation (17) yields

$$- \int_A \left\{ [(f-z)T]' + \frac{\partial \sigma_{xz}}{\partial z} \right\} z \delta w \, \mathrm{d}A \Big|_{x=0}^{x=l} + \int_y \int_x \frac{\partial (z\sigma_{xz})}{\partial x} \delta w \, \mathrm{d}x \, \mathrm{d}y \Big|_{z=-d}^{z=d}$$

$$- \int_x \int_A \frac{\partial \sigma_{xz}}{\partial x} \delta w \, \mathrm{d}A \, \mathrm{d}x + \int_x \{(K - I)T'' + 2T'K' + TK\} \delta w \, \mathrm{d}x. \tag{20}$$

Finally, substituting equations (19) and (20) into equation (17) and integrating over the cross-section A, we have

$$\int_x \{[(K - I - L_1 + K_1)T'' + (2K' - 2L_3 - L_2 + K_2)T' + (K'' - L_4 - L_5)T]$$

$$- \rho A \dot{P}\} \delta w \, \mathrm{d}x + \int_A \left\{ [(f-z)T]'(\varphi - z) + (\varphi - z) \frac{\partial \sigma_{xz}}{\partial z} \right\} \delta w \, \mathrm{d}A \Big|_{x=0}^{x=l}$$

$$- \int_y \int_x \frac{\partial ((\varphi - z)\sigma_{xz})}{\partial x} \delta w \, \mathrm{d}x \, \mathrm{d}y \Big|_{z=-d}^{z=d}. \tag{21}$$

2.3.5. *Boundary force terms*

The last two terms in equation (8) represent the boundary conditions for the ends and the lateral surfaces of the beam. They are incorporated with the other boundary condition terms as follows

(1) *Lateral surfaces.* We assume that the lateral surfaces of the beam are free of external traction, i.e., $\bar{g}_i = 0$ on these surfaces. This assumption comes from the relationship between g_i and σ_{ij} (given by Cauchy's formula),

$$g_i = v_j \sigma_{ij}, \tag{22}$$

where v_i is the unit outer normal vector. Since v_x and v_y are zero and v_z is 1 on the lateral surface, equation (22) becomes:

$$g_x = \sigma_{xz}, \qquad g_y = 0, \qquad g_z = 0. \tag{23}$$

Accordingly, the condition that the lateral surfaces are traction-free corresponds to the requirement that $\sigma_{xz} = 0$ on these surfaces.

The boundary force term in equation (8) over the lateral surface is

$$\int_x \int_y [(0 - \sigma_{xz})|_{z=-d}\delta u + (0 + \sigma_{xz})|_{z=d}\delta u]\,\mathrm{d}x\,\mathrm{d}y = \int_x \int_y (-\sigma_{xz})\delta u\,\mathrm{d}x\,\mathrm{d}y\Big|_{z=-d}^{z=d}. \tag{24}$$

Integrating by parts over x yields

$$\left[\left(\int_y (\varphi - z)(-\sigma_{xz})\delta w\,\mathrm{d}y\right)\Big|_{x=0}^{x=l} - \int_x \int_y \frac{\partial\{(\varphi - z)(-\sigma_{xz})\}}{\partial x}\delta w\,\mathrm{d}x\,\mathrm{d}y\right]\Big|_{z=-d}^{z=d}. \tag{25}$$

The second term in equation (25) cancels the last term in equation (21). The remaining force term in equation (21) can be integrated by parts over z and results in a term that is cancelled by the first term in equation (25). The remaining term turns out to be the end condition:

$$\int_A \{[(f - z)T]'(\varphi - z) + \sigma_{xz}\}\delta w\,\mathrm{d}A\Big|_{x=0}^{x=l}. \tag{26}$$

(2) *End surfaces.* We have $v_x = -1$ and $+1$ at the ends $x = 0$ and l, respectively. According to equation (22), g_x reduces to $\pm\sigma_{xx}$ and g_z to $\pm\sigma_{xz}$ at $x = 0$ and $x = l$, respectively. The external tractions at the ends, $\bar{g}_i$, are prescribed as $\bar{X}$ and $\bar{Z}$. The force boundary term in equation (8) is therefore

$$\int_A \{(\bar{X} - \sigma_{xx})\delta u + (\bar{Z} - \sigma_{xz})\delta w\}\,\mathrm{d}A|_{x=l} + \int_A \{(\bar{X} + \sigma_{xx})\delta u + (\bar{Z} + \sigma_{xz})\delta w\}\,\mathrm{d}A|_{x=0}, \tag{27}$$

Combining equation (26) with equation (27) and substituting the relations (6), the boundary force terms become

$$\begin{aligned}
&\left[\left\{\int_A (\varphi - z)\bar{X}\,\mathrm{d}A - T(I + L_1 - K - K_1)\right\}\delta w' \right.\\
&\quad \left. + \left\{\int_A \bar{Z}\,\mathrm{d}A + T'(I + L_1 - K - K_1) + T(L_3 - K')\right\}\delta w\right]_{x=l}\\
&\quad + \left[\left\{\int_A (\varphi - z)\bar{X}\,\mathrm{d}A + T(I + L_1 - K - K_1)\right\}\delta w' \right.\\
&\quad \left. + \left\{\int_A \bar{Z}\,\mathrm{d}A - T'(I + L_1 - K - K_1) + T(L_3 - K')\right\}\delta w\right]_{x=0}.
\end{aligned} \tag{28}$$

2.3.6. *Boundary displacement terms*

With $\bar{u}$ and $\bar{w}$ as the prescribed displacements at the ends $x = 0, l$, the boundary displacement terms in equation (8) are

$$\int_A \{(u - \bar{u})\delta\sigma_{xx} + (w - \bar{w})\delta\sigma_{xz}\}\,\mathrm{d}A|_{x=l} - \int_A \{(u - \bar{u})\delta\sigma_{xx} + (w - \bar{w})\delta\sigma_{xz}\}\,\mathrm{d}A|_{x=0}. \tag{29}$$

Substituting for u and σ_{xx} from equation (6) and integrating over the cross-section yields

$$\left[\left\{(I + L_1 - K - K_1)w' - \int_A \bar{u}(f - z)\,\mathrm{d}A\right\}\delta T + [(w - \bar{w})A\delta\sigma_{xz}]\right]_{x=l}$$
$$-\left[\left\{(I + L_1 - K - K_1)w' - \int_A \bar{u}(f - z)\,\mathrm{d}A\right\}\delta T + [(w - \bar{w})A\delta\sigma_{xz}]\right]_{x=0}. \quad (30)$$

2.3.7. *Derivation of equation of motion*

Finally, the variational terms (11), (14), (15) and (21) are substituted into equation (8), along with the boundary terms (28) and (30). Since the variations δw, δP, δS and δT are independent, each quantity multiplied by the corresponding variation must equal zero. This leads, from equation (11), to

$$S = Q_1(x)w'', \quad (31)$$

where

$$Q_1 = (I + L_1 - K - K_1)/(I - 2K + L). \quad (32)$$

The above equation shows that $(I - 2K + L)$ necessarily differs from zero. Therefore, from equation (14),

$$T = ES. \quad (33)$$

From equation (15),

$$P = \dot{w}. \quad (34)$$

From equation (21),

$$(K - I - L_1 + K_1)T'' + (2K' - 2L_3 - L_2 + K_2)T' + (K'' - L_4 - L_5)T - \rho A\dot{P} = 0. \quad (35)$$

Equation (35) can be rewritten in terms of the displacement w by substituting S, T and P from equations (31), (33) and (34). This leads to the equation of motion

$$E(I + L_1 - K - K_1)Q_1 w'''' + E[2(I + L_1 - K - K_1)Q_1'$$
$$+ (2L_3 + L_2 - K_2 + 2K')Q_1]w''' + E[(I + L_1 - K - K_1)Q_1''$$
$$+ (2L_3 + L_2 - K_2 - 2K')Q_1' + (L_4 + L_5 - K'')Q_1]w'' + \rho A\ddot{w} = 0. \quad (36)$$

Clearly, if there is no crack, the functions L, L_1, K and K_1 are zero, and Q_1 becomes unity. The equation of motion reduces to that of a uniform Bernoulli–Euler beam.

2.3.8. *Derivation of boundary conditions*

For specified displacements, the boundary conditions are obtained by equating the surface integral (28) to zero when u and w are prescribed on the boundary.

For specified forces, the boundary conditions are obtained by equating the surface integral (30) to zero when the external forces T and σ_{xz} are prescribed on the boundary.

For example, let us consider a cantilevered beam with a fixed end at $x = 0$. The virtual displacements δu (i.e., $\delta w'$) and δw must vanish at $x = 0$, implying that δT and $\delta\sigma_{xz}$ are arbitrary. With $\bar{u} = 0$ and $\bar{w} = 0$, at $x = 0$, equation (30) gives

$$w = 0, \qquad w' = 0. \quad (37)$$

At $x = l$, the external forces $\bar{X}$ and $\bar{Z}$ are zero, and equation (28) gives

$$T(I + L_1 - K - K_1) = 0 \quad (38)$$

and

$$T'(I + L_1 - K - K_1) + T(L_3 - K') = 0. \tag{39}$$

Since $(I + L_1 - K - K_1)$ differs from zero, the above two equations imply that $w'' = 0$ (from $T = 0$) and that $w''' = 0$ (from $T' = 0$).

2.3.9. *Calculation of the constant m*

The above cracked beam theory is based on the stress and strain distributions, equations (1) and (2), and the slope of the in-plane displacement, equation (4). The stress (or strain) distribution is characterized by the crack function f, with the parameters α and m defining the stress profiles in the x and z directions. The parameter α is evaluated in section 3, in a least square sense. Since the stress along the z direction is assumed to be linear, its decay rate m can be estimated from the condition that the same bending moment is carried by the cracked beam and the uncracked beam at the crack section:

$$\int_A (-zEw'')z \, dA = \int_{A_c} (-z + f(x_c, z))ES(x_c, t)(z + a/2) \, dA, \tag{40}$$

where A_c is the cross-sectional area at the crack tip ($x = x_c$) and the left side of equation (40) is for the uncracked beam.

At the crack-tip section, we have, from equations (3), (31) and (32),

$$f(x_c, z) = z - m(z + a/2), \qquad Q_1(x_c) = 1/m, \tag{41, 42}$$

$$S(x_c, t) = Q_1(x_c)w''(x_c, t). \tag{43}$$

Substituting the above results into equation (40) and integrating over the cross-section, we find that

$$m = I/[I_r + (a/2)I_c], \tag{44}$$

where

$$I_r = \int_{A_c} z^2 \, dA, \qquad I_c = \int_{A_c} z \, dA, \tag{45, 46}$$

are the second and first moments of the area of the reduced section with respect to z (the origin is at the centroid of the uncracked section).

3. APPLICATION TO BEAMS WITH RECTANGULAR CROSS-SECTION

The cracked beam theory is applied to examine the modes of free vibration of simply supported and cantilevered beams with one single-edge crack. We consider a beam of rectangular cross-section of depth $2d$ and breadth $2b$, with one crack of depth a located at $x = x_c$. The constants and functions in equations (10), (18) and (44) are

$$I = 4bd^3/3, \qquad I_r = 2b[(d - a)^3 + d^3]/3, \qquad I_c = ab(a - 2d), \tag{47}$$

$$m = \frac{1}{1 + \frac{3}{4}(a/d)^2 - \frac{3}{2}(a/d) - \frac{1}{8}(a/d)^3}, \tag{48}$$

$$K = 0, \qquad K' = 0, \qquad K'' = 0, \tag{49}$$

$$L = (m - 1)I \exp(-2\alpha|x - x_c|/d), \tag{50}$$

$$L_1 = IC_1 \exp(-2\alpha|x - x_c|/d),$$

$$K_1 = IC_1 \exp(-\alpha|x - x_c|/d), \qquad C_1 = (1 - 1/m),$$

$$L_2 + L_3 = L_1', \qquad L_4 + L_5 = L_3' = \tfrac{1}{2}L_1'', \qquad L_2 = K_1'. \tag{51}$$

The modes of free vibration of the cracked beam are obtained by assuming simple harmonic motion of frequency, ω_c. Taking $w(x, t) = \hat{w}(x)\, e^{j\omega_c t}$ leads to

$$E(I + L_1 - K_1)Q_1\hat{w}'''' + E[2(I + L_1 - K_1)Q_1' + 2L_3 + L_2 - K_2)Q_1]\hat{w}''' + E[(I + L_1 - K_1)Q_1'' + (2L_3 + L_2 - K_2)Q_1' + (L_4 + L_5)Q_1]\hat{w}'' - \omega_c^2 \rho A \hat{w} = 0. \quad (52)$$

For an uncracked beam, Q_1 equals 1, and L_1, K_1, L_2, K_2, L_3, L_4 and L_5 equal 0. Thus, equation (52) reduces to the Bernoulli–Euler beam equation.

For a cracked beam, the continuity characteristics of the solution are altered by the crack: the solution has a continuous second derivative $\hat{w}''$ but only a piecewise continuous third derivative $\hat{w}'''$, with a jump at the crack-tip section (for details, see reference [9]). This weaker continuity of the solution significantly deteriorates the convergence of the discretization method used to approximate the normal modes in equation (52).

3.1. FREE VIBRATION OF A SIMPLY SUPPORTED BEAM WITH A MID-SPAN CRACK

The free modes of a simply supported beam with a single-edge crack at mid-span are studied. Since Q_1 in equation (52) is a function of the rate of stress decay, the latter cannot be determined by the above theory alone. Thus, to both validate the theoretical formulation and determine the stress decay rate α, numerical results are obtained first from a finite element analysis.

3.1.1. *Finite element mesh*

The finite element mesh, with four quarter-point rectangular elements to model the crack tip, is shown in Figure 2(a). Transition elements [17] are used above and below the crack-tip elements [18, 19] to capture the stress singularity which is assumed to cover the entire thickness of the beam. This mesh is designed to yield accurate results which rapidly converge as the mesh is refined, both for uncracked and cracked beams. It consists of 40 eight-noded, plane stress, two-dimensional elements, totalling 151 nodal points and 298 degrees of freedom. In Figure 2(a), the beam's slenderness ratio ($\equiv l/2d$) is equal to 20·0.

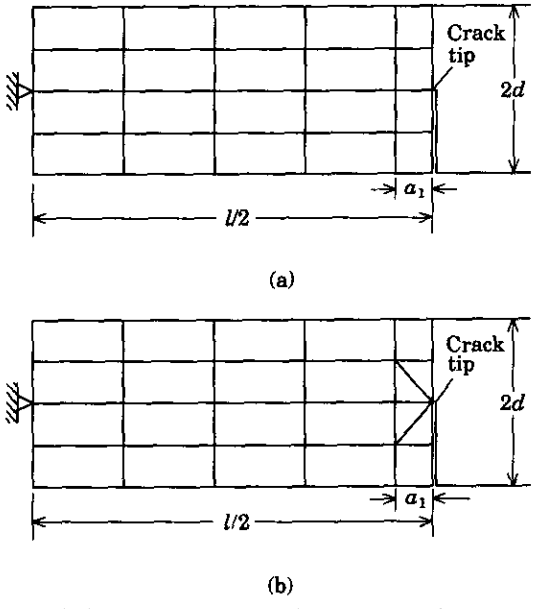

Figure 2. Finite element mesh for a simply supported beam containing a single-edge crack at mid-span ($x_c = l/2$): (a) rectangular elements; (b) triangular elements. $l/2d = 20$, $l/2a_1 = 24$.

TABLE 1

Natural frequency of uncracked and cracked beams (single crack)

Uncracked beam (natural frequency parameter $\bar{\beta} = \omega_c \sqrt{\rho A l^4 / EI}$)

	Galerkin solution ($N = 100$)†	Finite element (rectangular)	
	$\bar{\beta}$	$\bar{\beta}$	*SE*‡
First mode	9·8696	9·8461	1·04847
Second mode	39·4784	39·1003	16·68123
Third mode	88·8264	87·1909	82·71803

Cracked beam (first mode)

		Finite element			
	Galerkin solution ($\alpha = 1{\cdot}276$, $N = 100$)	Rectangular		Triangular	
CR	*FR*	*FR*	*SE*	*FR*	*SE*
0·1	0·98837	Not available			
0·2	0·97415	Not available			
1/4	0·96546	0·97119	0·95932	0·97238	0·96253
1/3	0·94716	0·94922	0·89884	0·95027	0·90145
1/2	0·88137	0·88294	0·73743	0·88742	0·74764
0·6	0·80080	Not available			
2/3	0·71410	Not available			

Cracked beam (second mode)

		Finite element			
	Galerkin solution ($\alpha = 1{\cdot}276$, $N = 100$)	Rectangular		Triangular	
CR	*FR*	*FR*	*SE*	*FR*	*SE*
0·1	0·99956	Not available			
0·2	0·99916	Not available			
1/4	0·99897	0·99998	16·68105	1·00001	16·68134
1/3	0·99868	1·00005	16·68397	1·00009	16·68438
1/2	0·99812	0·99969	16·67600	0·99972	16·67694
0·6	0·99761	Not available			
2/3	0·99697	Not available			

Cracked beam (third mode)

		Finite element			
	Galerkin solution ($\alpha = 1{\cdot}276$, $N = 100$)	Rectangular		Triangular	
CR	*FR*	*FR*	*SE*	*FR*	*SE*
0·1	0·98886	Not available			
0·2	0·97573	Not available			
1/4	0·96796	0·97270	68·14161	0·97372	68·41354
1/3	0·95225	0·95379	61·33226	0·95462	61·49821
1/2	0·90260	0·90296	47·60207	0·90607	48·38150
0·6	0·85403	Not available			
2/3	0·81323	Not available			

† N = number of terms in the Galerkin expansion.
‡ *SE* = strain energy.

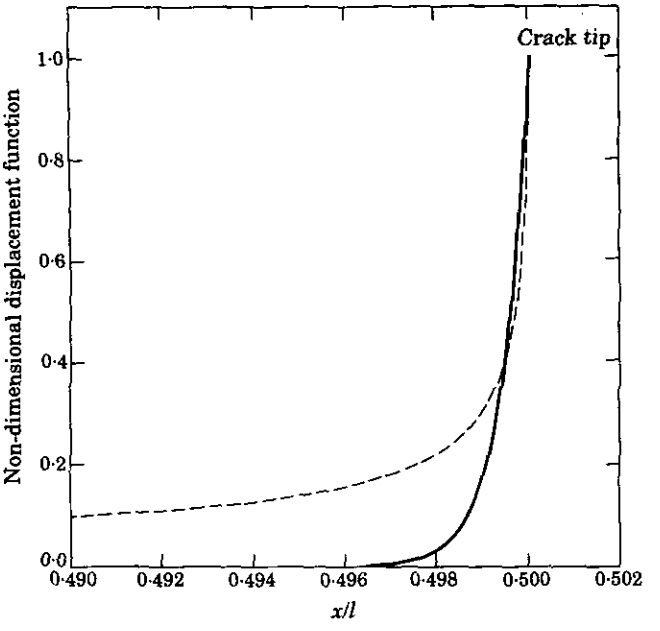

Figure 3. Displacement function profile for a simply supported beam ($l/2d = 20$) with a single crack at mid-span ($XC = 0{\cdot}5$): – – – –, $1/\sqrt{r}$ (r is the distance from the crack tip); ——, displacement function ($\beta = 21{\cdot}94$).

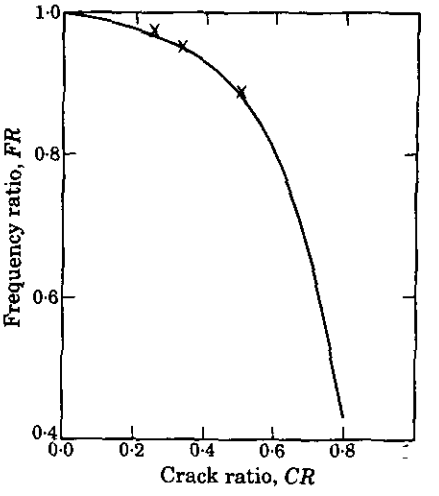

Figure 4. Fundamental natural frequency in terms of crack depth. Theoretical and finite element results are shown for a simply supported beam ($l/2d = 20$) with a single-edge crack at mid-span ($x_c = l/2$). +, Finite element (rectangular); ×, finite element (triangular); ——, Galerkin solution, $\alpha = 1{\cdot}276$, $N = 100$.

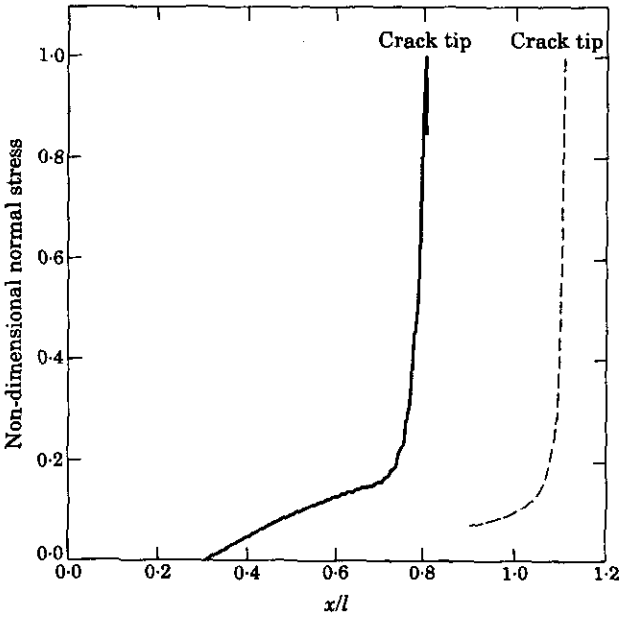

Figure 5. Normal stress profile in the first mode for a simply supported beam with a single crack ($CR = 1/3$) at mid-span ($XC = 0{\cdot}5$). The origin of each curve is shifted to avoid overlap: – – – –, $1/\sqrt{r}$ (r is the distance from the crack tip); ——, Galerkin solution, $N = 100$ ($\alpha = 1{\cdot}276$).

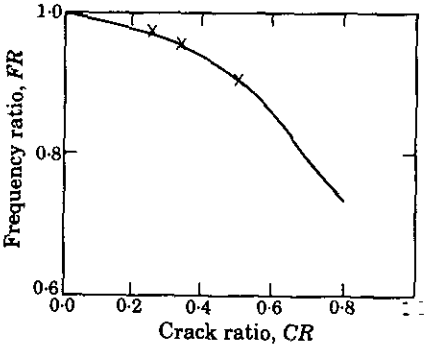

Figure 6. Third natural frequency in terms of crack depth. Theoretical and finite element results are shown for a simply supported beam ($l/2d = 20$) with a single-edge crack at mid-span ($x_c = l/2$). +, Finite element (rectangular); ×, finite element (triangular); ——, Galerkin solution, $\alpha = 1{\cdot}276$, $N = 100$.

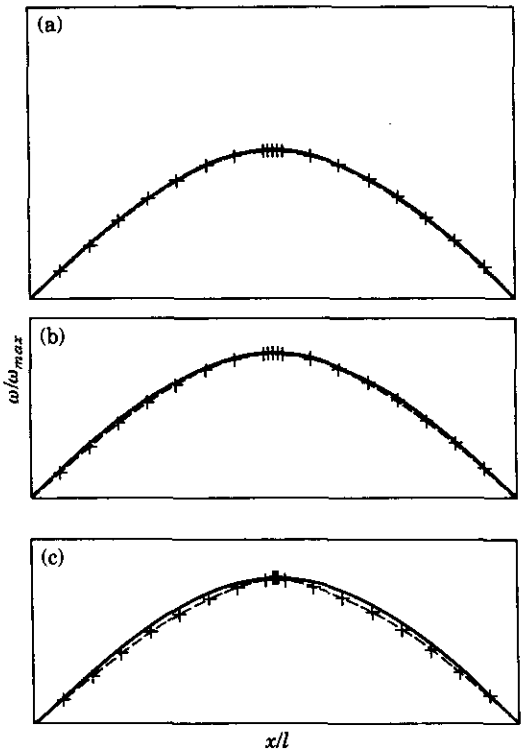

Figure 7. First mode shape of a simply supported beam ($l/2d = 20$) with a single-edge crack at mid-span ($x_c = l/2$). Galerkin and finite element results are shown for various crack ratios: (a) $CR = \frac{1}{4}$, (b) $CR = \frac{1}{3}$, (c) $CR = \frac{1}{2}$. +, Finite element; – – –, Galerkin solution, $\alpha = 1{\cdot}276$, $N = 100$; ——, uncracked beam.

The 16 nodal displacements for each element are the in-plane displacements u and w at each node. The size of the quarter-point elements at the crack tip is chosen to capture the effect of the singularity. The elements cover 1/24 of the beam's length in the axial direction, such that they extend over nearly all the stress concentration. Quarter-point elements of various sizes were tested, such that the elements' length was much smaller or much greater than the range of the stress concentration. Crack-tip elements that were too narrow or too wide led to considerable errors. It was demonstrated numerically that the finite element mesh shown in Figure 2(a) gives a nearly optimal result for the present problem. Since no special procedure is needed to compute the stiffness and mass matrices for the distorted crack tip element, any general purpose finite element code can be used.

An alternative finite element mesh, which essentially replaces every rectangular quarter-point element in Figure 2(a) by two triangular quarter-point elements, is illustrated in Figure 2(b). The mesh consists of 44 elements, 157 nodal points and 310 degrees of freedom. All the results obtained by the triangular elements are very close to those given by the rectangular ones.

To validate the finite element model, the lowest three natural frequencies of the uncracked beam were compared to Bernoulli–Euler theory results. As shown in Table 1, the finite element frequencies are, respectively, 0·24, 0·96 and 1·8% lower than the Bernoulli–Euler results. Since there are no geometrical assumptions for the finite element formulation, the natural frequencies are expected to be lower, especially for the higher modes.

3.1.2. *Finite element results*

The modes of vibration were computed for crack depths of $\frac{1}{4}$, $\frac{1}{3}$ and $\frac{1}{2}$ of the total beam thickness. The natural frequencies, as shown in Table 1 and Figures 3 and 4, are presented in the form of the frequency ratio (FR), the ratio of the frequency of the cracked beam to that of the uncracked beam, *vs.* the crack depth ratio (CR), the ratio of the depth of the crack to the beam thickness. The first three mode shapes for cracked beams with crack ratios of $\frac{1}{4}$, $\frac{1}{3}$, and $\frac{1}{2}$ are plotted in Figures 5–7 and compared to the modes of the uncracked beam. The changes in the first and third mode shapes are significant for large crack ratios only ($CR > \frac{1}{4}$). The second mode shape is unaffected by the crack for all ratios examined. This is because the crack is located at mid-span, where compressive or tensile stresses equal zero in the even vibration modes. Therefore, for a beam pinned at both ends, a single-edge crack at the middle will not affect the even, antisymmetrical modes of vibration.

It has been shown in reference [9] that for a pair of cracks, the strain energy in the odd modes decreases, while in the even modes it remains unchanged. Similarly, for single-edge cracked beams, it is shown in Table 1 that the strain energy in the first and third modes decreases as the crack depth increases and that the strain energy for the second mode remains unchanged. This is consistent with the above frequency and mode shape observations.

3.1.3. *Galerkin solution*

We seek a Galerkin approximate solution to the continuous eigenvalue problem, equation (52), by expanding the transverse deflection in a series in the infinitely differentiable modes of the uncracked beam [9],

$$\hat{w}(\xi) = \sum_{i=1}^{N} a_i \sin(i\pi\xi). \tag{53}$$

Because the modes of the cracked beam have a discontinuous third derivative, their Galerkin expansion requires a large number of terms N to satisfy the convergence criterion

$$\max_{i=1,2,3} \left| \frac{\Delta\omega_i^N}{\omega_{ci}^N} \right| < \epsilon, \tag{54}$$

where $\Delta\omega_i^N$ is the change in the ith frequency from the N-term to the $(N+1)$-term calculation, ω_{ci}^N is the N-term estimate of the ith frequency of the cracked beam, and ϵ is a small real number. For all cases presented in this paper, 100 terms were necessary to achieve convergence with $\epsilon = 2{\cdot}0 \times 10^{-5}$.

Substituting equation (53) into equation (52) and applying the Galerkin procedure, we obtain a discrete eigenvalue problem of size N in the generalized co-ordinates, a_i:

$$[K_c]\mathbf{a} - \omega_c^2[M_c]\mathbf{a} = \mathbf{0}, \tag{55}$$

where

$$[M_c] = (\rho Al/2)[I] \tag{56}$$

is the mass matrix, $[I]$ is the identity matrix, the vector $\mathbf{a} = [a_1, a_2, \ldots, a_N]^T$, and

$$\begin{aligned}[K_c] = (EI\pi^4/l^3) \int_0^1 \{ & i^2j^2(1 + \bar{L}_1(\xi) - \bar{K}_1(\xi))Q_1(\xi) \sin i\pi\xi \sin j\pi\xi \\ & + (l/2\pi)ij^2[(\bar{L}_2(\xi) - \bar{K}_2(\xi))Q_1(\xi)] \cos i\pi\xi \sin j\pi\xi \\ & + (l/2\pi)i^2j[(\bar{L}_2(\xi) - \bar{K}_2(\xi))Q_1(\xi)] \sin i\pi\xi \cos j\pi\xi \} \, d\xi \end{aligned} \tag{57}$$

is the stiffness matrix. The functions $\bar{L}(\xi)$, $\bar{L}_1(\xi)$, $\bar{K}_1(\xi)$, $\bar{L}_2(\xi)$, $\bar{K}_2(\xi)$ and $Q_1(\xi)$ are defined as

$$\bar{L}(\xi) = C\exp(-2\alpha P), \qquad L_1(\xi) = C_1\exp(-\alpha P)\exp(-2\beta P),$$

$$\bar{K}_1(\xi) = C_1\exp(-2\beta P), \qquad \bar{L}_2(\xi) = \bar{L}_1(\xi)\frac{\mathrm{d}\exp(-2\beta P)}{\mathrm{d}\xi},$$

$$\bar{K}_2(\xi) = \mathrm{d}\bar{K}_1(\xi)/\mathrm{d}\xi, \qquad Q_1(\xi) = \frac{1+\bar{L}_1(\xi)-\bar{K}_1(\xi)}{1+\bar{L}(\xi)}, \qquad P = |\xi - \tfrac{1}{2}|/d. \tag{58}$$

3.1.4. *Determination of the neutral surface shift constant* β

The rate of neutral surface shift β is obtained by fitting the displacement function $\varphi(x, z)$, in a least square sense, best with the normalized theoretical stress decay function $1/\sqrt{r}$, where the variable r is the distance from the crack tip. As it is shown in Figure 3, the least square fit of the displacement function with the function $1/\sqrt{r}$ determined the value of parameter β to be 21·94.

3.1.5. *Determination of the stress decay constant* α

Once the number of terms yielding satisfactory convergence is determined, the rate of stress decay α is obtained by fitting the natural frequencies calculated by Galerkin's method best with the finite element results, in a least square sense. Only the fundamental frequency is considered for simplicity.

The fundamental frequency drop in terms of crack depth is shown in Figure 4 and Table 1. The least square fit of the 120-term Galerkin solution with the finite element results determined the rate of stress decay α to be 1·276. As we expect, the corresponding normal stress distribution shown in Figure 5 reaches a maximum at the cracked section and decays proportionally to $1/\sqrt{r}$.

Figure 6 and Table 1 show the variation of the third natural frequency with the crack ratio. Similarly to the fundamental mode, there is excellent agreement between Galerkin and finite element results for crack ratios smaller than 1/2. Crack ratios larger than 1/2 were not considered, as failure would occur before such a value is reached.

3.1.6. *Examination of the mode shapes*

The mode shapes obtained by the Galerkin and finite element formulations are compared in Figures 7–9. One observes that the Galerkin results are consistently in good agreement with the finite element ones.

The prediction of the crack's location and depth based upon only one mode could be misleading. For instance, by reviewing only the data for the second mode, as given in Table 1 and Figure 8, one would conclude that the beam is not damaged. This implies that different modes viewed separately might yield different predictions of damage, i.e., crack position and depth. Moreover, from Figures 7(c) and 9(c), the effect on the third mode is more severe than on the first. Therefore, it is expected that a multi-mode analysis is needed to identify the position and size of a crack.

3.2. FREE VIBRATION OF CRACKED CANTILEVERED BEAMS

The above cracked beam theory is applied to a cantilevered beam (see Figure 10) with a single-edge crack. However, the numerical integration of the free bending modes of the uncracked beam (required to generate the mass and stiffness coefficients in the Galerkin procedure) causes a computer overflow, because these modes involve hyperbolic functions and many modes are required. Therefore, the Galerkin procedure with 100 terms is impractical in the cantilevered case.

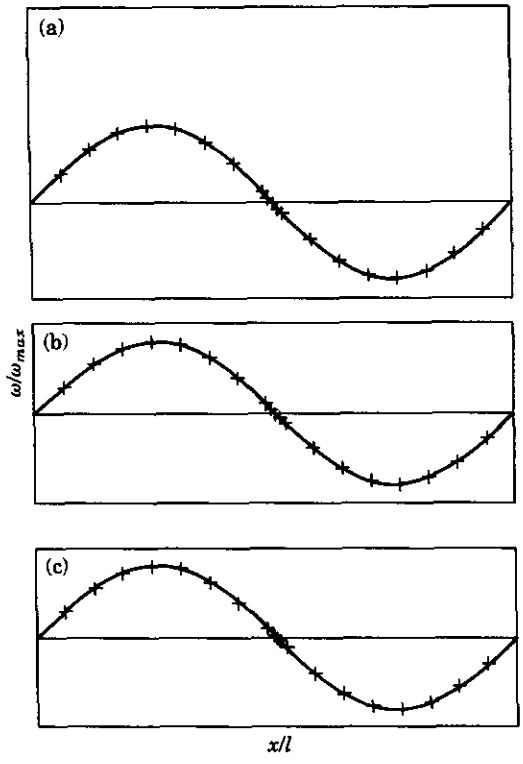

Figure 8. Second mode shape of a simply supported beam ($l/2d = 20$) with a single-edge crack at mid-span ($x_c = l/2$). Galerkin and finite element results are shown for various crack ratios: (a) $CR = \frac{1}{4}$, (b) $CR = \frac{1}{3}$, (c) $CR = \frac{1}{2}$. Key as Figure 7.

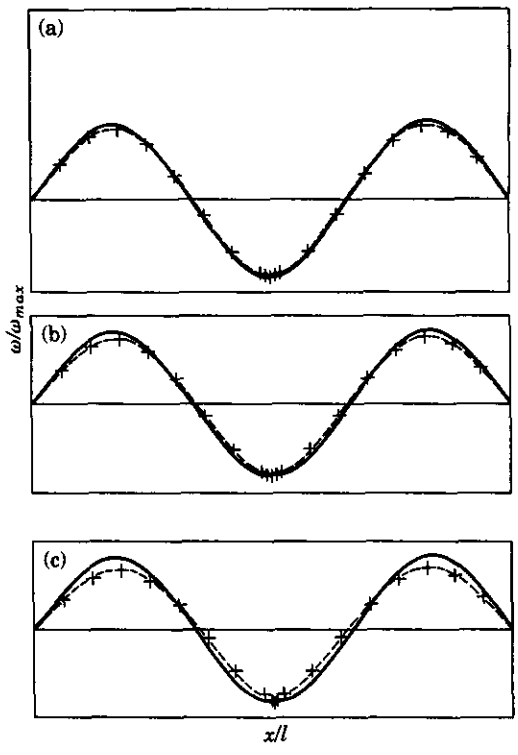

Figure 9. Third mode shape of a simply supported beam ($l/2d = 20$) with a single-edge crack at mid-span ($x_c = l/2$). Galerkin and finite element results are shown for various crack ratios: (a) $CR = \frac{1}{4}$, (b) $CR = \frac{1}{3}$, (c) $CR = \frac{1}{2}$. Key as in Figure 7.

3.2.1. *Local Ritz method*

To circumvent this problem, a local Rayleigh–Ritz approach which uses a piecewise fit to the deflection shape is presented. The displacement, $\hat{w}(x)$, is approximated by piecing cubic polynomials, each defined over only a portion of the structure, or sub-beam. The coefficients of the polynomials can be determined uniquely in terms of the displacements

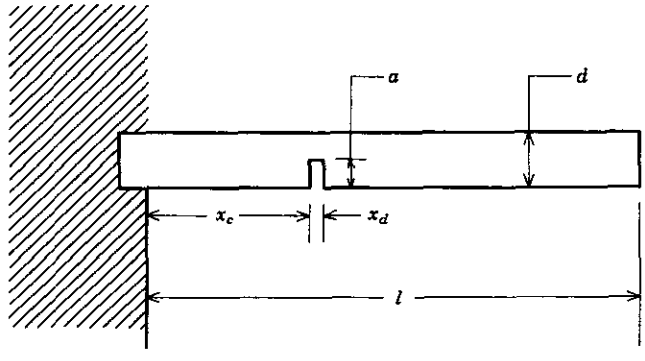

Figure 10. Geometry of the experimental cantilevered beam with a single-edge crack at x_c, $l/d = 25{\cdot}64$, $x_d/l = 0{\cdot}0035$, $CR = a/d$ (from reference [20]).

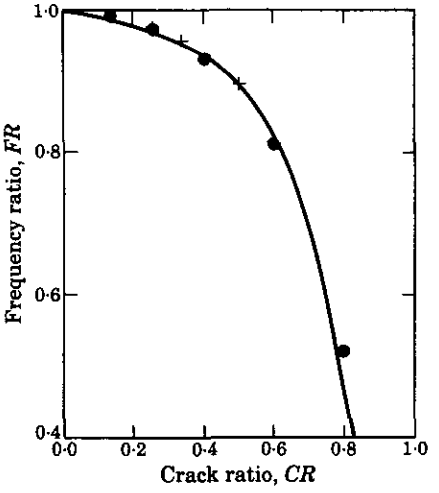

Figure 11. Fundamental natural frequency in terms of crack depth. Theoretical, finite element and experimental results are shown for a cantilevered beam ($l/2d = 25{\cdot}64$) with a single-edge crack at $x_c = 0{\cdot}2l$ ($XC = 0{\cdot}2$). +, Finite element (rectangular); ●, experiment, Wendtland [20]; ——, local Ritz method, $\alpha = 1{\cdot}276$, 50 sub-beams.

and slopes at the end points. The displacement at a point within the ith sub-beam is approximated as

$$\hat{w}_i(\eta) = \mathbf{F}^{\mathrm{T}}(\eta)\mathbf{u}_i, \qquad 0 \leqslant \eta \leqslant l_s, \tag{59}$$

where $\mathbf{F} = (F_1, F_2, F_3, F_4]^{\mathrm{T}}$ is a vector of prescribed (shape) functions of position and $\mathbf{u}_i$ is a vector of end displacements and slopes for the ith sub-beam. The shape functions $(F_j)_{j=1,\ldots,4}$ are listed in Appendix A. This piecewise polynomial interpolation amounts to a finite element solution of the cracked beam differential equation (52). In this analysis, a local Rayleigh–Ritz model with four shape functions, M identical sub-beams, $M + 1$ nodes, and $2M$ DOF is used.

The free vibration eigenvalue problem is expressed as

$$[K_e]\mathbf{u} - \omega_c^2[M_e]\mathbf{u} = \mathbf{0}, \tag{60}$$

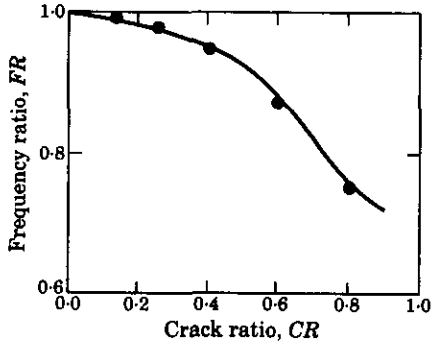

Figure 12. Third natural frequency in terms of crack depth. Theoretical and experimental results are shown for a cantilevered beam ($l/2d = 25{\cdot}64$) with a single-edge crack at $x_c = 0{\cdot}3l$ ($XC = 0{\cdot}3$). Key as Figure 11.

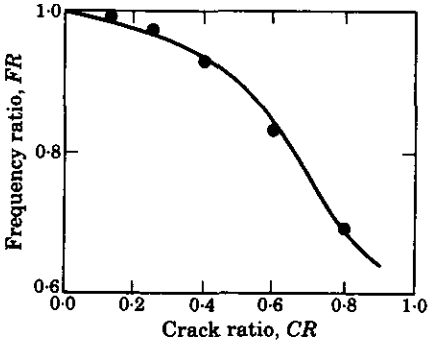

Figure 13. Third natural frequency in terms of crack depth. Theoretical and experimental results are shown for a cantilevered beam ($l/2d = 25{\cdot}64$) with a single-edge crack at $x_c = 0{\cdot}7l$ ($XC = 0{\cdot}7$). Key as Figure 11.

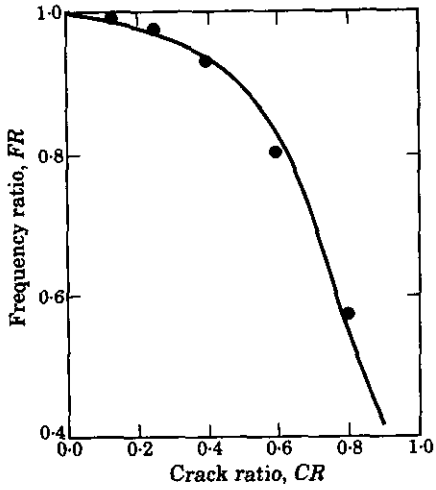

Figure 14. Second natural frequency in terms of crack depth. Theoretical and experimental results are shown for a cantilevered beam ($l/2d = 25{\cdot}64$) with a single-edge crack at $x_c = 0{\cdot}55l$ ($XC = 0{\cdot}55$). Key as Figure 11.

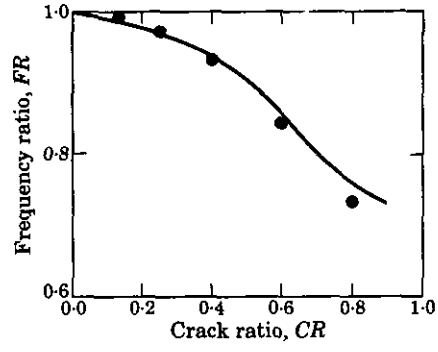

Figure 15. Fourth natural frequency in terms of crack depth. Theoretical and experimental results are shown for a cantilevered beam ($l/2d = 25{\cdot}64$) with a single-edge crack at position $x_c = 0{\cdot}8l$ ($XC = 0{\cdot}8$). Key as Figure 11.

where $\mathbf{u}$ is the vector of nodal displacements, and $[K_e]$ and $[M_e]$ are $(2M \times 2M)$ stiffness and mass matrices for the entire beam. The assemblage process to obtain $[K_e]$ and $[M_e]$ is symbolically described by

$$(\mathbf{u}, [K_e], [M_e]) = \sum_{i=1}^{M} (\mathbf{u}_i, [k_i], [m_i]), \tag{61}$$

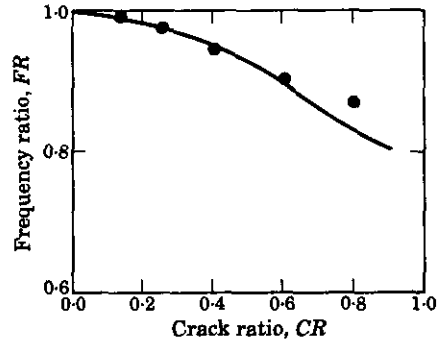

Figure 16. Fifth natural frequency in terms of crack depth. Theoretical and experimental results are shown for a cantilevered beam ($l/2d = 25{\cdot}64$) with single-edge crack at position $x_c = 0{\cdot}6l$ ($XC = 0{\cdot}6$). Key as Figure 11.

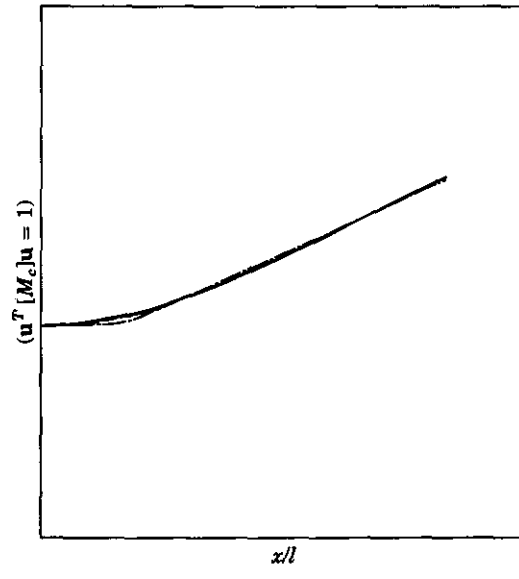

Figure 17. First mode shape of a cantilevered beam ($l/2d = 25{\cdot}64$) with a single-edge crack at $x_c = 0{\cdot}2l$ ($XC = 0{\cdot}2$). Ritz's result is shown for various crack ratios: ——, $CR = 0{\cdot}0$; – – – –, $CR = 0{\cdot}13$; — – —, $CR = 0{\cdot}5$; — · —, $CR = 0{\cdot}8$.

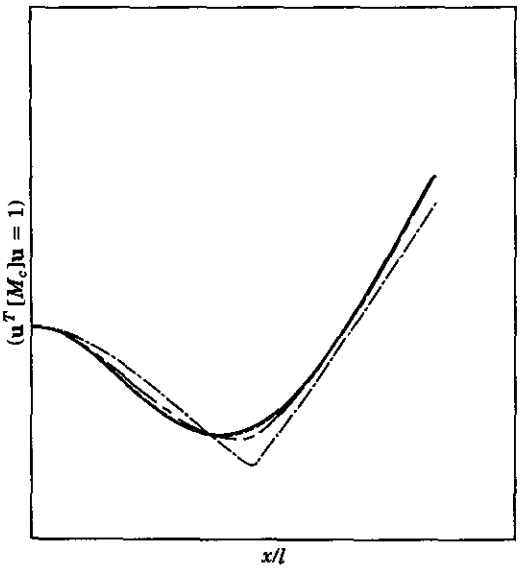

Figure 18. Second mode shape of a cantilevered beam ($l/2d = 25{\cdot}64$) with a single-edge crack at $x_c = 0{\cdot}55l$ ($XC = 0{\cdot}55$). Ritz's result is shown for various crack ratios: ——, $CR = 0{\cdot}0$; – – – –, $CR = 0{\cdot}13$; — – —, $CR = 0{\cdot}5$; — · —, $CR = 0{\cdot}8$.

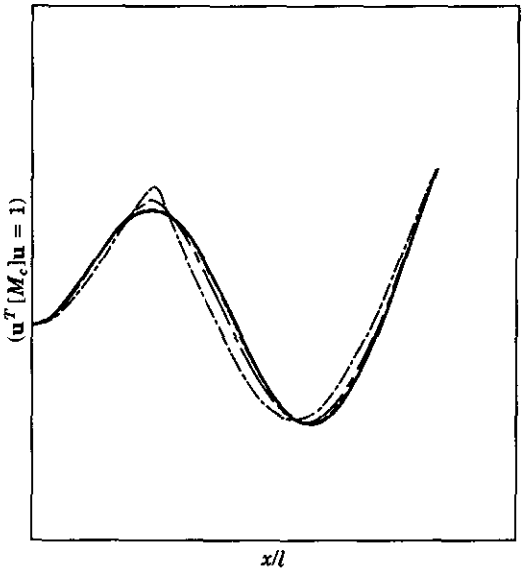

Figure 19. Third mode shape of a cantilevered beam ($l/2d = 25{\cdot}64$) with a single-edge crack at $x_c = 0{\cdot}3l$ ($XC = 0{\cdot}3$). Ritz's result is shown for various crack ratios: ——, $CR = 0{\cdot}0$; – – – –, $CR = 0{\cdot}13$; — – —, $CR = 0{\cdot}5$; — · —, $CR = 0{\cdot}8$.

where $\mathbf{u}_i$, $[k_i]$ and $[m_i]$ are the nodal displacements, stiffness and mass matrices, respectively, for the ith sub-beam, and the summation is over all M sub-beams. The (4×4) mass and stiffness matrices of the ith sub-beam in the local co-ordinate system are

$$[m_i] = \int_0^{l_i} \mathbf{F}^{\mathrm{T}}\mathbf{F}\, d\eta \tag{62}$$

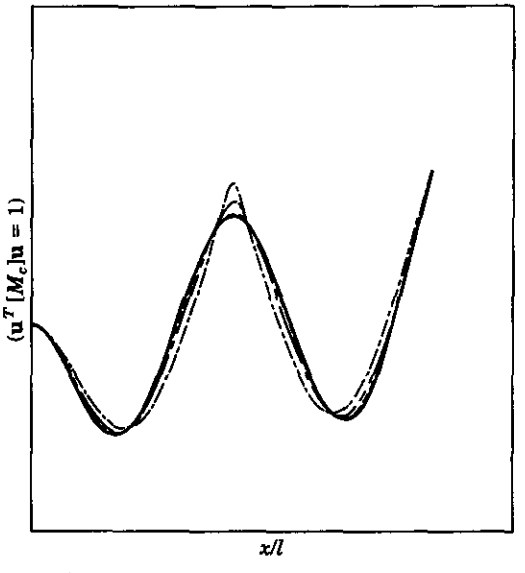

Figure 20. Fourth mode shape of a cantilevered beam ($l/2d = 25{\cdot}64$) with a single-edge crack at $x_c = 0{\cdot}5l$ ($XC = 0{\cdot}5$). Ritz's result is shown for various crack ratios: ——, $CR = 0{\cdot}0$; – – – –, $CR = 0{\cdot}13$; — – —, $CR = 0{\cdot}5$; — · —, $CR = 0{\cdot}8$.

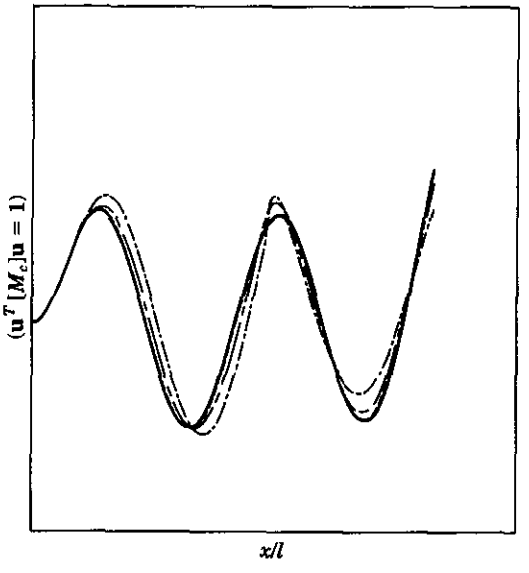

Figure 21. Fifth mode shape of a cantilevered beam ($l/2d = 25{\cdot}64$) with a single-edge crack at $x_c = 0{\cdot}7l$ ($XC = 0{\cdot}7$). Ritz's result is shown for various crack ratios: ——, $CR = 0{\cdot}0$; – – – –, $CR = 0{\cdot}13$; — – —, $CR = 0{\cdot}5$; — · —, $CR = 0{\cdot}8$.

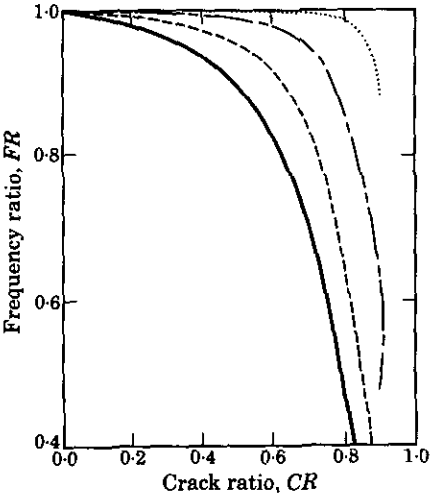

Figure 22. Fundamental natural frequency in terms of crack depth for a cantilevered beam ($l/2d = 25{\cdot}64$). Ritz's result is shown for various crack positions: ——, $XC = 0{\cdot}2$; – – – –, $XC = 0{\cdot}4$; — – —, $XC = 0{\cdot}6$; · · · ·, $XC = 0{\cdot}8$.

and

$$[k_i] = (EI/\rho A)\int_0^{l_i} \{(1{\cdot}0 + \bar{L}_1(\eta) - \bar{K}_1(\eta))Q_1(\eta)\mathbf{B}^{\mathrm{T}}\mathbf{B} + (1/l)[(\bar{L}_2(\eta) - \bar{K}_2(\eta))Q_1(\eta)]\mathbf{B}\mathbf{1}^{\mathrm{T}}\mathbf{B} + (1/l)[(\bar{L}_2(\eta) - \bar{K}_2(\eta))Q_1(\eta)]\mathbf{B}^{\mathrm{T}}\mathbf{B}\mathbf{1}\}\,\mathrm{d}\eta, \tag{63}$$

where $\mathbf{B1} = (\mathrm{d}/\mathrm{d}\eta)\mathbf{F}$ and $\mathbf{B} = (\mathrm{d}^2/\mathrm{d}^2\eta)\mathbf{F}$.

The value of α was determined to be 1·267 by a least square fit with the finite element results (see Figure 11). The eigenvalue problem, equation (60), was then solved for an increasing number of sub-beams, M, until a frequency convergence test was satisfied. The

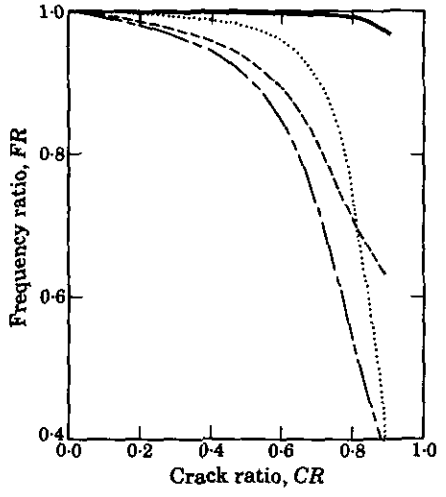

Figure 23. Second natural frequency in terms of crack depth for a cantilevered beam ($l/2d = 25{\cdot}64$). Ritz's result is shown for various crack positions: ——, $XC = 0{\cdot}2$; – – – –, $XC = 0{\cdot}4$; — – —, $XC = 0{\cdot}6$; · · · ·, $XC = 0{\cdot}8$.

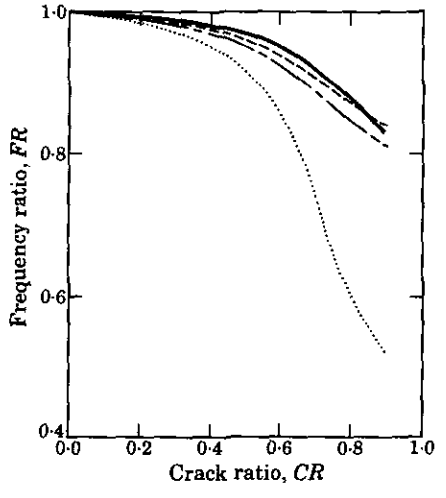

Figure 24. Third natural frequency in terms of crack depth for a cantilevered beam ($l/2d = 25{\cdot}64$). Ritz's result is shown for various crack positions: ——, $XC = 0{\cdot}2$; – – – –, $XC = 0{\cdot}4$; — – —, $XC = 0{\cdot}6$; · · · ·, $XC = 0{\cdot}8$.

convergence criterion used was similar to that for the Galerkin approach, equation (54), except that the number of sub-beams, M, was increased instead of the number of uncracked modes, N. At least 50 sub-beams ($M \geqslant 50$) were needed in the local Rayleigh–Ritz procedure to satisfy the convergence criterion ($\epsilon = 2{\cdot}0 \times 10^{-5}$) for the fundamental mode.

3.2.2. *Experimental verification*

The effects of cracks on the natural frequencies of beams have been studied experimentally by Wendtland [20] and Wendtland and Wiederuh [21]. In reference [20], the cracks were obtained by sawing cuts of width 0·0035 times the length of the beam (see Figure 10), and the lowest five natural frequencies were measured for various crack ratios and positions.

We obtained the lowest five eigenfrequencies for rectangular beams with cracks at $x_c/l = XC = 0{\cdot}2$, 0·3, 0·55, 0·6, 0·7 and 0·8. Selected theoretical results are compared with the experimental data obtained by Wendtland [20] in Figures 11–16. Observe that our theoretical frequencies correlate very closely with the experimental ones for crack ratios up to 0·8. This excellent comparison confirms the validity of our theory.

3.2.3. *Examination of the mode shapes*

The first five mode shapes of cracked beams with crack ratios of 0·13, 0·5 and 0·8 and various locations are compared to those of an uncracked beam in Figures 17–21. Observe the severe deformation near the crack tip for large cracks, which could be used to detect crack position.

3.2.4. *Effects of crack position on the dynamical response*

We examined the effect of crack position on the sensitivity of natural frequencies and mode shapes of a cantilevered beam with a single-edge crack. The first bending frequency is shown in Figure 22 as a function of the crack ratio for four crack positions, $XC = 0{\cdot}2$, 0·4, 0·6 and 0·8. The drop in frequency is far greater for cracks near the clamped end, while the frequency is almost unchanged when the crack is located near the free end. This result can be explained by noting that the bending moment is distributed heavily near the fixed end for the fundamental mode, leading to a severe loss in bending stiffness due to the crack. However, the drop in frequency is different in the higher modes. The solid curves in Figures 23 and 24 show that the second and third frequencies are comparatively much less affected than the fundamental one for $CR = 0{\cdot}2$, but are strongly affected for other crack locations: $XC = 0{\cdot}6$ and 0·8 for the second and third modes, respectively. In other words, the frequency drop is greatest for a crack located where the bending moment is largest. Clearly, the sensitivity to cracks depends highly on the mode number and the crack position.

Several observations can be made from the above discussion. First, for a given mode, the effects on the bending frequency and mode shape become more severe as the crack depth grows. Second, for a certain crack ratio, the crack position strongly affects the dynamic behavior of a cracked beam. Third, if the position of the crack is known information, one specific mode may be sufficient to obtain accurate results in the crack identification problem. However, if the crack position is unknown, the uniqueness and accuracy of the identification process becomes questionable. In general, the more modes are used for crack identification, the more accurate and reliable the result will be.

4. CONCLUSIONS

A formulation for the flexural motion of a Bernoulli–Euler beam containing a single-edge crack is presented. It is based on two key kinematic assumptions, made to

satisfy the compatibility requirements in the vicinity of the crack. First, the stress concentration near the crack tip is accounted for by introducing a crack function into the beams' compatibility relations. Second, a function is introduced that modifies the in-plane displacement and its slope to avoid the discontinuity in the slope of the neutral axis at the single crack.

The equation of motion and associated boundary conditions are derived. The validity of the theory is established by examining two different sets of boundary conditions. The analytical solutions show excellent agreement with both experimental results and finite element predictions. The effects of cracks on frequency and mode shape are found to be very sensitive to crack location and mode number.

The present theory could be extended easily to beams with non-rectangular cross-section and account for shear deformation (Timoshenko beam). Other future work includes the development of an inverse analysis procedure to identify the crack properties from dynamical measurements.

ACKNOWLEDGMENTS

The authors are grateful to Professor John Taylor (The University of Michigan) for his valuable comments and expert suggestions. This work was partly supported by NSF Grant No. MSM-8700820.

REFERENCES

1. T. G. Chondros and A. D. Dimarogonas 1980 *Journal of Sound and Vibration* **69**, 531–538. Identification of cracks in welded joints of complex structures.
2. A. D. Dimarogonas and G. Massouros 1981 *Engineering Fracture Mechanics* **15**, 439–444. Torsional vibration of a shaft with a circumferential crack.
3. A. D. Dimarogonas and C. A. Papadopoulos 1983 *Journal of Sound and Vibration* **91**, 583–593. Vibration of cracked shafts in bending.
4. P. Gudmundson 1983 *Journal of the Mechanics and Physics of Solids* **31**, 329–345. The dynamic behaviour of slender structures with cross-sectional cracks.
5. C. A. Papadopoulos and A. D. Dimarogonas 1987 *Ingenieur-Archiv* **57**, 257–266. Coupling of bending and torsional vibration of a cracked Timoshenko shaft.
6. P. Cawley and R. D. Adams 1979 *Journal of Strain Analysis* **14**, 49–57. The location of defects in structures from measurements of natural frequencies.
7. P. Cowley and R. D. Adams 1979 *ASMT Paper* **79**-*DET*-46. Defect location in structures by a vibration technique.
8. S. Christides and A. D. S. Barr 1984 *International Journal of the Mechanical Sciences* **26**, 639–648. One-dimensional theory of cracked Bernoulli–Euler beams.
9. M. H. Shen and C. Pierre 1990 *Journal of Sound and Vibration* **138**, 115–134. Natural modes of Bernoulli–Euler beams with symmetric cracks.
10. L. B. Freund 1972 *Journal of Applied Mechanics* **39** *Transactions of the American Society of Mechanical Engineers* **94**, Series E, 601–602. The initial wave front emitted by a suddenly extending crack in an elastic solid.
11. L. B. Freund 1972 *Journal of the Mechanics and Physics of Solids* **20**, 129–152. Crack propagation in an elastic solid subjected to general loading.
12. L. B. Freund 1974 *Journal of the Mechanics and Physics of Solids* **22**, 137–146. Crack propagation in an elastic solid subjected to general loading.
13. S. Bodner 1973 *Journal of the Mechanics and Physics of Solids* **21**, 1–8. Stress waves due to fracture of glass in bending.
14. L. B. Freund and G. Herrmann 1975 *Journal of Applied Mechanics* **43**, 112–116. Dynamic fracture of a beam or plate in pure bending.
15. G. R. Irwin 1960 in *Structural Mechanics* (P. C. Goodier and N. J. Hoff, editors). New York: Pergamon Press.

16. P. C. PARIS and G. C. SIH 1965 *Fracture Toughness and Its Applications ASME STP-***381**, 30. Stress analysis of cracks.
17. P. P. LYNN and A. R. INGRAFFEA 1977 *International Journal of Numerical Methods in Engineering* **11**, 1031–1036. Transition elements to be used with quarter-point crack-tip elements.
18. R. D. HENSHELL and K. G. SHAW 1975 *International Journal of Numerical Methods in Engineering* **9**, 454–509. Crack tip finite element are unnecessary.
19. R. S. BARSOUM 1976 *International Journal of Numerical Methods in Engineering* **10**, 25–37. On the use of isoparametric finite element in linear fracture mechanics.
20. D. WENDTLAND 1972 *Ph.D. Thesis, University of Karlsruhe*. Änderung der biegeeigenfrequenzen einer idealisierten Schaufel durch Risse.
21. D. WENDTLAND and E. WIEDERUH 1974 *Forschung in Ingenieurwesen* **40**, 60–66. Änderungen der Torsionseigenfrequenzen von Turbomaschinenschaufeln durch Risse.

APPENDIX A: SHAPE FUNCTIONS

$$F_1(\eta) = 1 - 3(\eta/l_s)^2 + 2(\eta/l_s)^3, \qquad F_2(\eta) = \eta - 2(\eta^2/l_s) + (\eta^3/l_s^2), \tag{A1}$$

$$F_3(\eta) = 3(\eta/l_s)^2 - 2(\eta/l_s)^3, \qquad F_4(\eta) = -(\eta^2/l_s) + (\eta^3/l_s^2),$$

$$l_s = l/M, \qquad 0 \leqslant \eta \leqslant l_s.$$

APPENDIX B: NOMENCLATURE

a	crack depth	$[m_i]$	element mass matrix
a_i	ith generalized co-ordinate amplitude	M	number of sub-beams in the local Ritz method
A	beam cross-sectional area	$[M_e]$	global mass matrix
b	half breadth of rectangular beam	N	number of terms in the Galerkin expansion
CR	$\equiv a/2d$, crack ratio	S	strain function
d	half depth of rectangular beam	T	stress function
E	Young's modulus of elasticity	u_i	$= u, v, w$, displacement components
$f(x, z)$	crack function	$\mathbf{u}$	vector of nodal displacements in local Ritz method
FR	$= \omega_c/\omega_{uc}$, frequency ratio	V	total volume
$H(\cdot)$	unit step function	$w(x, t)$	bending deflection
I	cross-sectional area moment of inertia	$\hat{w}(x)$	bending deflection amplitude
$[k_i]$	element stiffness matrix	x_c	crack position
$[K_e]$	global stiffness matrix	XC	$\equiv x_c/l$
K	$\equiv \int_A zf \, dA$	α	stress decay constant
K_1	$\equiv \int_A z\varphi \, dA$	β	neutral surface shift constant
K_2	$\equiv \int_A z\varphi' \, dA$	δ_{ij}	Kronecker's delta, $=1$ for $i = j$ and $=0$ for $i \neq j$
$\bar{K}_1$	$\equiv K_1/I$	ρ	density
$\bar{K}_2$	$\equiv K_2/I$	ϵ_{ij}	strain tensor component
l	length of beam	σ_{ij}	stress tensor component
l_s	$\equiv l/M$, length of sub-beam	ω_c	free vibration natural frequency (cracked beam)
L	$\equiv \int_A f^2 \, dA$	ω_{uc}	free vibration natural frequency (uncracked beam)
L_1	$\equiv \int_A f\varphi \, dA$	ξ	$\equiv x/l$
L_2	$\equiv \int_A f\varphi' \, dA$	$\varphi(x, z)$	displacement function
$\bar{L}$	$\equiv L/I$	η	position co-ordinate along a sub-beam
$\bar{L}_1$	$\equiv L_1/I$	$\cdot$	$\equiv \partial/\partial t$
$\bar{L}_2$	$\equiv L_2/I$	$'$	$\equiv \partial/\partial x$
L_3	$\equiv \int_A f'\varphi \, dA$		
L_4	$\equiv \int_A f''\varphi \, dA$		
L_5	$\equiv \int_A f'\varphi' \, dA$		
Q_1	integrated crack function		
m	stress magnification factor		